

Observation of a robust peak in the glue function of the high- T_c cuprates in the 50-60 meV range.

E. van Heumen,¹ E. Muhlethaler,¹ A.B. Kuzmenko,¹ D. van der Marel,¹ H. Eisaki,² M. Greven,³ W. Meevasana,³ and Z.X. Shen³

¹*Département de Physique de la Matière Condensée, Université de Genève, quai Ernest-Ansermet 24, CH1211, Genève 4, Switzerland*

²*Nanoelectronics Research Institute, National Institute of Advanced Industrial Science and Technology, Tsukuba, Japan*

³*Department of Physics, Applied Physics, and Stanford Synchrotron Radiation Laboratory, Stanford University, Stanford, CA 94305*

We take advantage of the connection between the free carrier optical conductivity and the glue function in the normal state, to reconstruct from the infrared optical conductivity the glue-spectrum of ten different high- T_c cuprates revealing a robust peak in the 50-60 meV range and a broad continuum at higher energies for all measured charge carrier concentrations and temperatures up to 290 K. We observe an intriguing correlation between the doping trend of the experimental glue spectra and the critical temperature.

The theoretical approaches to the high T_c pairing mechanism in the cuprates are divided in two main groups: According to the first school electrons form pairs due to a retarded attractive interaction mediated by virtual bosonic excitations in the solid[1, 2, 3, 4, 5]. These bosons can be lattice vibrations, fluctuations of spin-polarization, electric polarization or charge density. The second school concentrates on a pairing-mechanism entirely due to the non-retarded Coulomb interaction[6] or so-called Mottness[7]. Indeed, optical experiments have found indications for mixing of high and low energy degrees of freedom when the sample enters into the superconducting state[8, 9, 10, 11].

An indication that both mechanisms are present was obtained by Maier, Poilblanc and Scalapino[12], who showed that the 'anomalous' selfenergy associated with the pairing has a small but finite contribution extending to an energy as high as U , demonstrating that the pairing-interaction is, in part, non-retarded. They arrived at the conclusion, that "for the cuprate materials, the relative weight of the retarded and nonretarded interaction remains an open question. Thus, the continuing experimental search for a pairing glue in the cuprates is important and will play an essential role in determining the origin of the high- T_c pairing interaction." Aforementioned glue can be expressed with the help of the density of states of these bosons multiplied by the electron-boson coupling, $\alpha^2 F(\omega)$ for phonons and $I^2 \chi(\omega)$ for spinfluctuations, in this Letter represented by the general symbol $\tilde{\Pi}(\omega)$. An important consequence of the electron-boson coupling is, that the energy of the quasi-particles relative to the Fermi level, ξ , is renormalized, and their lifetime becomes limited by inelastic decay processes involving the emission of bosons. The corresponding energy shift and the inverse lifetime, *i.e.* the real and imaginary parts of the self-energy, are expressed as the convolution of the 'glue-function' $\tilde{\Pi}(\omega)$ with a kernel $K(\xi, \omega, T)$ describing

the thermal excitations of the glue and the electrons[13]

$$\Sigma(\xi) = \int K(\xi, \omega, T) \tilde{\Pi}(\omega) d\omega \quad (1)$$

In the absence of a glue and of scattering off impurities the effect of applying an AC electric field to the electron gas is to induce a purely reactive current response, characterized by the imaginary optical conductivity $4\pi\sigma(\omega) = i\omega_p^2/\omega$, where the plasma frequency, ω_p , is given by the (partial) f-sum rule for the conduction electrons. The effect of coupling the electrons to bosonic excitations is revealed by a finite, frequency dependent dissipation, which can be understood as arising from processes whereby a photon is absorbed by the simultaneous creation of an electron-hole pair and a boson. As a result, the expression for the optical conductivity in the normal state, $4\pi\sigma(\omega) = i\omega_p^2/\{\omega + 2\Sigma_{opt}(\omega)\}$, now contains a memory function[14] equivalent to an 'optical self-energy'. A particularly useful aspect of this representation is that $\Sigma_{opt}(\omega)$ follows in a straightforward way from the experimental optical conductivity. The optical self-energy is related to the single particle self-energies by the expression[15]

$$\frac{2\Sigma_{opt}(\omega)}{\omega} = \left\{ \int \frac{f(\xi) - f(\xi + \omega)}{\omega + \Sigma^*(\xi) - \Sigma(\xi + \omega)} d\xi \right\}^{-1} - 1 \quad (2)$$

The central assumption in the above is the validity of the Landau Fermi-liquid picture for the normal state. The aforementioned strong coupling analysis is therefore expected to work best on the overdoped side of the cuprate phase diagram, where the state of matter appears to become increasingly Fermi liquid like. If antiferromagnetism is necessary to obtain the insulating state in the undoped parent compounds, as has been argued based on the doping trends of the Drude spectral weight[16], the strong coupling analysis may in principle be relevant for the entire doping range studied. However, in the limit of strong interactions aforementioned formalism needs to

be extended, *e.g.* with vertex corrections, and eventually breaks down. We therefore *define* the function $\tilde{\Pi}(\omega)$ as the *effective* quantity which, in combination with Eqs. 1 and 2, returns the exact value of $\Sigma_{opt}(\omega)$ for each frequency. Defined in this way $\tilde{\Pi}(\omega)$ captures *all* correlation effects regardless whether the system is a Fermi-liquid or not. This becomes increasingly relevant when the doping is lowered below optimal doping.

Here we take advantage of the connection between the temperature and frequency dependent conductivity in the normal state and the glue-spectrum to test experimentally the consequences of the standard approach, to check the internal consistency of it, and to determine the range of doping where internal consistency is obtained. For a d-wave superconductor, the momentum dependence is essential to understand the details of the pairing. This, of course, is difficult to handle for optical spectroscopy which is inherently a momentum integrated probe. Nevertheless, optical spectra provide the important information on the energy scale of the bosons involved and on the doping and temperature evolution. We use a standard least squares routine to fit a histogram representation of $\tilde{\Pi}(\omega)$ to our experimental infrared spectra. The quantity $\tilde{\Pi}(\omega)$ is shown in Fig. 1 for optimally doped $\text{HgBa}_2\text{CuO}_{4+\delta}$ (Hg-1201)[17] for $T = 290$ K, together with the optical self energies calculated from this function at three different temperatures. For 290 K the theoretical curve runs through the data points, reflecting the full convergence of the numerical fitting routine. It is interesting to notice, that the shoulder in the experimental data at 100 K is reproduced by the same $\tilde{\Pi}(\omega)$ function as the one used to fit the 290 K data. In other words, the strong temperature dependence of the experimental optical spectra is entirely due to the Fermi and Bose factors of Eqs. 1 and 2. It can be excluded that the shoulder at 80 meV is due to the pseudo-gap, since a gap is certainly absent for temperatures as high as 290 K. The shoulder is therefore entirely due to coupling of the electrons to a mode at approximately 60 meV. On the other hand, the considerable sharpening of this feature for temperatures lower than 100 K finds a natural explanation in the opening of a gap, as illustrated in the inset of Fig. 1. This example confirms the close correspondence between the features in $\Sigma_{opt}(\omega)$ and in $\tilde{\Pi}(\omega)$ pointed out in Ref. [18]. In particular the broad maximum in $\Sigma_{opt}(\omega)$ has its counterpart in the high intensity region of $\tilde{\Pi}(\omega)$ terminating at 290 meV.

As summarized in Fig. 2, we have analyzed previously published optical spectra of 6 different samples belonging to different families of materials, *i.e.* optimally doped Hg-1201[17] and $\text{Bi}_2\text{Sr}_2\text{Ca}_2\text{Cu}_3\text{O}_{10+\delta}$ (Bi-2223)[11], as well as four $\text{Bi}_2\text{Sr}_2\text{CaCu}_2\text{O}_{8+\delta}$ (Bi-2212) crystals [9, 10] with different hole concentrations. In addition, we analyzed new data for four $\text{Bi}_2\text{Sr}_2\text{Cu}_2\text{O}_{6+\delta}$ (Bi-2201) crystals with different hole concentrations[19].

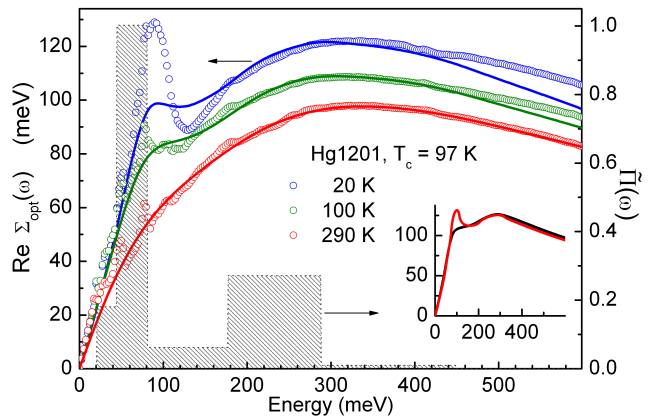


FIG. 1: Experimental optical self energy of $\text{HgBa}_2\text{CuO}_{4+\delta}$ for 3 selected temperatures (open circles). The solid curve at 290 Kelvin is obtained from a fit of $\tilde{\Pi}(\omega)$, shown as the dashed surface. The solid curves at 100 K and 20 K were calculated with the same $\tilde{\Pi}(\omega)$ function corresponding to 290 Kelvin. This proves that the self energy feature between 80 and 100 meV (a shoulder at 100 K and a peak at 20 K) is caused by the prominent peak in $\tilde{\Pi}(\omega)$ at approximately 60 meV. The sharpening of this feature at low temperature is due to the superconducting gap, an aspect not captured by Eq. 2 and therefore not reproduced in the calculated solid curves. In the inset the gap-induced sharpening is illustrated by the optical self energy without (black) and with (red) a 15 meV superconducting gap, calculated using Allen's relation[15].

Excellent fits were obtained for all temperatures, but the $\tilde{\Pi}(\omega)$ spectra exhibit a significant temperature dependence, in particular at the low frequency side of the $\tilde{\Pi}(\omega)$ spectrum. Since all thermal factors contained in Eqs. 1 and 2 are, in principle, folded out by our procedure, the remaining temperature dependence of $\tilde{\Pi}(\omega)$ reflects the thermal properties of the 'glue-function' itself. Such temperature dependence is a direct consequence of the peculiar DC and far infrared conductivity, in particular the T -linear DC resistivity and ω/T scaling of $T\sigma(\omega, T)$ at optimal doping[20]. For the highest doping levels both $\tilde{\Pi}(\omega)$ and its temperature dependence diminish, which is an indication that a Fermi liquid regime is approached. The most strongly underdoped sample, Bi-2201-UD0, exhibits an upturn of the imaginary part of the experimental optical self-energy for $\omega \rightarrow 0$. This aspect of the data can not be reproduced by the strong coupling expression, resulting in an artificial and unphysical peak at $\omega \approx 0$ of the fitted $\tilde{\Pi}(\omega)$ function.

We observe two main features in the glue-function: A robust peak at 50-60 meV and a broad continuum. The upper limit of $\tilde{\Pi}(\omega)$ is situated around approximately 300 meV for optimally doped single layer Hg1201, and for the bilayer and trilayer samples. Interestingly the continuum extends to the highest energies (550 meV for the single-layer samples and 400 meV for the bilayer) for the

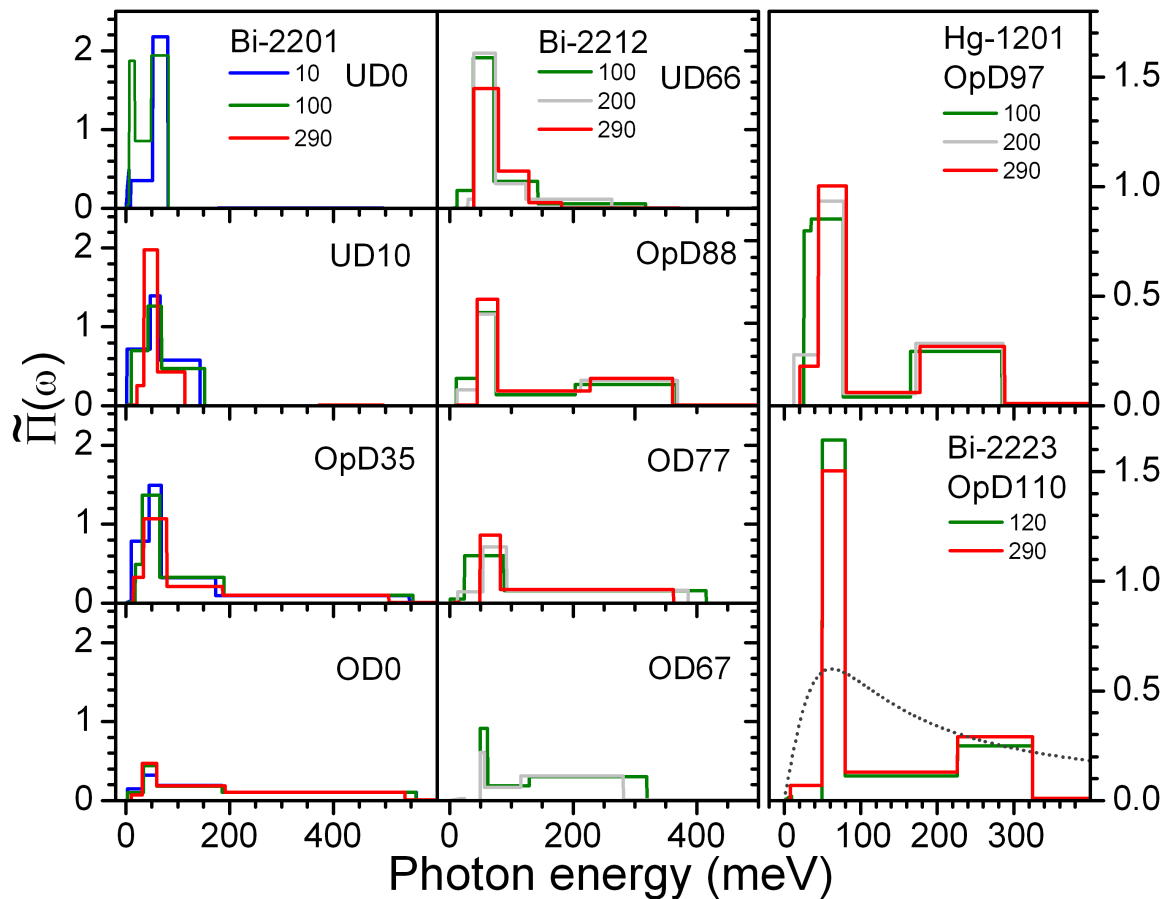


FIG. 2: Electron-boson coupling function $\tilde{\Pi}(\omega)$ for Bi-2201 at four different charge carrier concentrations (10 K, 100 K, 290 K), Bi-2212 at four charge carrier concentrations, and optimally doped Bi-2223 and Hg-1201 (100 K, 200 K, 290 K). The dotted curve in the lower right panel represents the spin-fluctuation model[3, 18].

x		0.09	0.11	0.16	0.22	0.11	0.16	0.20	0.21	0.16	0.16
T_c	K	0	10	35	0	66	88	77	67	110	97
$\hbar\omega_p$	eV	1.75	1.77	1.92	1.93	2.36	2.35	2.45	2.33	2.43	2.10
$\hbar\tilde{\omega}$	meV	-	70	81	103	92	124	116	154	101	81
λ		-	2.96	2.96	1.41	2.65	2.14	1.40	0.97	2.18	1.85

TABLE I: Strong coupling parameters of the ten compounds. The hole-doping is indicated on the first line. From left to right: Bi2201 (columns 1 to 4), Bi2212 (columns 5 to 8), Bi2223 (8th column) and Hg1201 (column 10). The definition of $\tilde{\omega}$ is $\ln(\tilde{\omega}) = 2\lambda^{-1} \int_0^\infty \omega^{-1} \tilde{\Pi}(\omega) \ln(\omega) d\omega$.

weakly overdoped samples, whereas the continuum of the strongly doped bilayer sample extends to only 300 meV. There is also a clear trend of a contraction of the continuum to lower energies when the carrier concentration is reduced. Taken together this doping trend suggests a possible relation of the glue-function to a quantum critical point at a doping concentration slightly higher than optimal doping[20, 21]. Hence, part of the glue function has an energy well above the upper limit of the phonon

frequencies in the cuprates (~ 100 meV). Consequently the high energy part of $\tilde{\Pi}(\omega)$ reflects in one way or another the strong coupling between the electrons themselves. The coupling constant is obtained from the relation $\lambda = 2 \int_0^\infty \tilde{\Pi}(\omega)/\omega d\omega$. The result (see Table I) shows a strong and systematic increase of λ for decreasing hole concentration, which probably requires a theoretical treatment beyond the strong coupling expansion outlined in the introduction.

The most prominent feature, present in all spectra reproduced in Fig. 2, is a peak corresponding to an average frequency of 55 meV. Perhaps the most striking aspect of this peak is the fact that its energy is practically independent of temperature (up to room temperature) and sample composition. Moreover, the intensity and width are essentially temperature independent. While our results confirm by and large the observations of Hwang *et al.* in the pseudo-gap phase[22, 23], the persistence of the 50-60 meV peak to room temperature has not been reported before. This peak arises most likely from the same boson that is responsible for the 'kink' seen in angle resolved photoemission (ARPES) experiments

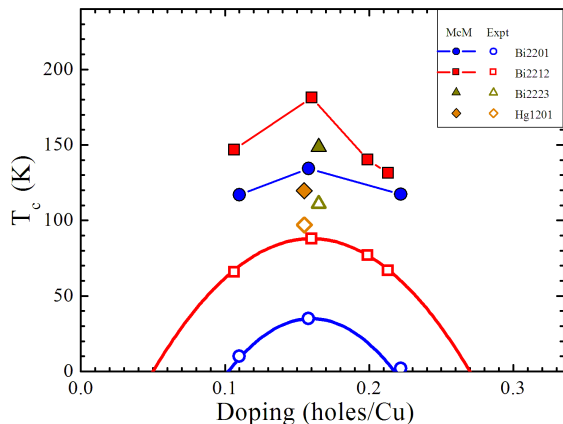


FIG. 3: Experimental critical temperature and T_c 's calculated from the McMillan formula using the experimentally measured $\tilde{\Pi}(\omega)$ of Fig. 2 at 290 Kelvin as input parameters.

along the nodal direction in k-space at approximately the same energy[24, 25, 26]. The peak-dip-hump structure in the tunneling spectra (STS)[27, 28, 29] has also been reported at approximately the same energy.

It is interesting to correlate our experimentally obtained glue-function with T_c . Millis, Varma and Sachdev[30] have shown, that, if $\tilde{\Pi}(\omega)$ can be decomposed in an s-wave and a d-wave channel and μ^* is considered negligibly small for the d-wave channel, then the critical temperature of the d-wave superconducting phase transition is $T_c \leq 0.83\tilde{\omega} \exp(-(1+\lambda)/\lambda)$ where $\tilde{\omega}$ is the logarithmic average of the frequency in $\tilde{\Pi}(\omega)$. We calculated this upper limit using the experimental values indicated in Table I. The T_c 's with this formula are in the 100-200 K range for all samples studied here, and, as shown in Fig. 3, they correlate with the experimentally observed doping trends of T_c for the single-layer and bilayer high- T_c materials. The calculated critical temperatures are about twice as large as the experimentally observed ones for the Bi2212 series, whereas in the Bi2201 single layer compounds T_c appears to be strongly suppressed as compared to the calculated value. The low value of T_c in single layer Bi2201 correlates with a relatively high intensity of $\tilde{\Pi}(\omega)$ below the 50-60 meV peak, and a very low intensity or absence of the 0.25 eV peak. In contrast, the three samples with the highest critical temperature, Bi2212 OpD88, Bi-2223 and Hg-1201, show the most pronounced weight at ~ 0.25 eV.

In summary, the $\tilde{\Pi}(\omega)$ spectrum obtained from the optical spectra of 10 different compounds using a strong coupling analysis, is observed to consist of two features: (i) a robust peak in the range of 50 to 60 meV and (ii) a doping dependent continuum extending to 0.3 eV for the samples with the highest T_c . Finally, we observe an intriguing correlation between the doping trend of the experimental glue spectra and the critical temperature.

We gratefully acknowledge C.M. Varma, D.J. Scalapino, J. Zaanen, A.V. Chubukov, C. Berthod, J.C. Davis, and A. Millis for stimulating discussions. This work is supported by the Swiss National Science Foundation through Grant No. 200020-113293 and the National Center of Competence in Research (NCCR) Materials with Novel Electronic PropertiesMaNEP.

APPENDIX

The inversion of Eq's 1 and 2 allows to extract $\tilde{\Pi}(\omega)$ from experimental data of the optical conductivity, or related optical spectra. The accuracy of the resulting $\tilde{\Pi}(\omega)$ spectrum is in practice limited by the convolution with thermal factors expressed by Eq's 1 and 2 [31]. Microscopic models giving roughly the same $\tilde{\Pi}(\omega)$ spectra, which differ however in the details of the frequency dependence of this quantity, may therefore provide fits to the directly measured optical quantities, such as infrared reflectance spectra, which at first glance look satisfactory, but the remaining discrepancies with the experimental spectra may nevertheless be of significant importance for the proper understanding of the optical data. It is therefore of crucial importance to test the 'robustness' of each fit with regard to the spectral shape of the $\tilde{\Pi}(\omega)$ function imposed by such models. This robustness can be tested by including in the fit-routine one or several 'oscillators' superimposed on the model function. When the model glue function provides a complete description of the electronic structure, adding extra oscillators will not result in an improvement of the quality of the fit. We have used this approach to test functional forms commonly used in the literature, in particular the marginal Fermi liquid (MFL) model [2] and the Millis-Monien-Pines (MMP) representation of the spin fluctuation spectrum[3]. We found that neither of these functional forms describe completely the experimental data.

In search of a more flexible form of $\tilde{\Pi}(\omega)$ we used a superposition of lorentzian oscillators and found that it could be used to describe all available experimental data in a consistent manner. The resulting $\tilde{\Pi}(\omega)$ functions and trends are equivalent to those in Fig. 2. From these initial tests we concluded that due to the thermal smearing expressed by Eq's 1 and 2 our $\tilde{\Pi}(\omega)$ spectra can only be determined with limited resolution. This lead us to the use of a histogram representation, where each block in the histogram represents a likelihood to find coupling to a mode with a well determined coupling strength. Only for the lowest frequency interval ($0 < \omega < \omega_1$) a triangular shape was used instead of a block, which is necessary to avoid problems with the convergence of the integral $\lambda = 2 \int_0^\infty \omega^{-1} \tilde{\Pi}(\omega) d\omega$. In practice the output generated by the fitting routine has low intensity in this first interval, and the triangles are therefore difficult to distinguish in Fig. 2.

To give an example: The block centered at 55 meV seen in the Hg-1201 sample in Fig. 2 has $\lambda \sim 1$ and a width of about 30 meV. Our histogram representation implies the presence of a coupling to one or several modes between 45 meV and 75 meV with an integrated coupling strength of 1. The histograms thus constitute the most detailed representation of $\tilde{\Pi}(\omega)$ given the precision of our experimental reflectivity and ellipsometry spectra.

Examples of experimental reflectivity data together with the fits are shown in Fig. 4 for a selection of representative data sets spanning the entire doping and temperature range. As the fitted curves are within the limits of the experimental noise, further reduction of χ^2 , while in principle possible by fitting the statistical noise of the data, can not improve the accuracy of the $\tilde{\Pi}(\omega)$ functions. Starting from a $\tilde{\Pi}(\omega)$ function we can calculate the opti-

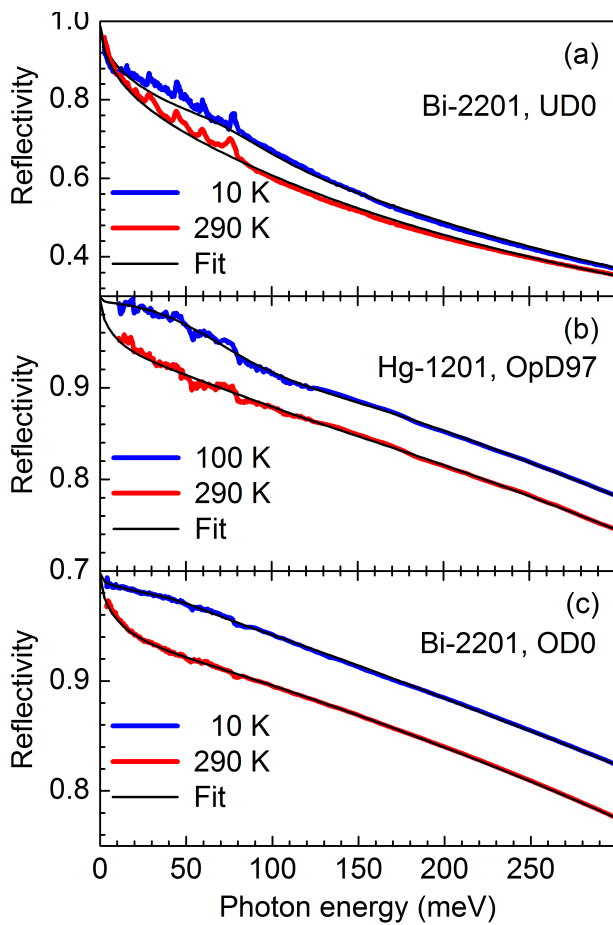


FIG. 4: Experimental reflectivity (red and blue lines) and fit curves (black lines) for selected samples and temperatures. (a): underdoped non-superconducting Bi-2201 (UD0). (b): optimally doped Hg-1201 with $T_c \approx 97$ K (OpD97) [17] (c): overdoped non-superconducting Bi-2201 (OD0). Weak sharp peaks, particularly visible for the strongly underdoped sample in panel (a) are due to transverse optical phonons, which we do not intend to fit.

cal conductivity, which in turn is fed into standard Fres-

nel expressions to calculate the experimentally measured quantities, *i.e.* reflectivity and ellipsometric parameters. The fitting routine is based on the Levenberg-Marquardt algorithm and uses analytical expressions for the partial derivatives of the reflectivity coefficient R , and the ellipsometric parameters ψ and Δ relative to the parameters describing the $\tilde{\Pi}(\omega)$ function. The algorithm is based around minimizing a functional χ^2 which is given by,

$$\chi^2 = \sum_{i=1}^N \left(\frac{R(\omega_i) - f(\omega_i, p_1, \dots, p_n)}{\sigma_i} \right)^2 \quad (3)$$

where $R(\omega_i)$ is an experimentally measured datapoint, $f(\omega_i, p_1, \dots, p_n)$ is the calculated value in this point based on parameters p_1, \dots, p_n and the difference between these two is weighed by the errorbar σ_i determined for $R(\omega_i)$. For a given set of reflectivity and ellipsometry data at one particular temperature, using a standard PC, the iteration takes about 3 hours until convergence is reached. Although the Levenberg-Marquardt least squares method is an extremely powerful method to find the minimum of χ^2 in a multidimensional parameter space it also has difficulties with finding the best solution to the non-linear problem Eq's 1 and 2. For each individual sample and temperature displayed in Fig. 5 several tests have been performed where in each test the optimization process was started from a different set of starting parameters to ensure that χ^2 has converged to the global minimum in parameter space. To give some idea of the robustness of our method we will here discuss one representative example: optimally doped Hg-1201.

The models are evaluated based on the minimum found for χ^2 . A comparison of Fig. 5 (a-d) shows that the MMP model describes better the optical data than the MFL model but that they give similar results if we add an extra oscillator to these models. Panels S5e-f show the model independent results mentioned above and are very similar to the modified MMP and MFL model. The models in these last two panels have the same χ^2 and the comparison in Fig. 5g shows that the histogram representation realistically expresses the uncertainty in the position of the low energy peak, while the correspondence between the features in both models remains excellent. It is interesting that the model with two oscillators is described by 6 parameters, while the histogram representation uses 12 parameters. The fact that the fit-routine adjusts the latter 12 parameters in such a manner as to produce in essence the two oscillator lineshape, proves that the features represented in the righthand panel of Fig. 5 are realistic. An extensive discussion of this analysis is provided in Ref. [32].

[1] D.J. Scalapino, E. Loh, J.E. Hirsch, *Phys. Rev. B* **34**, 8190 (1986).

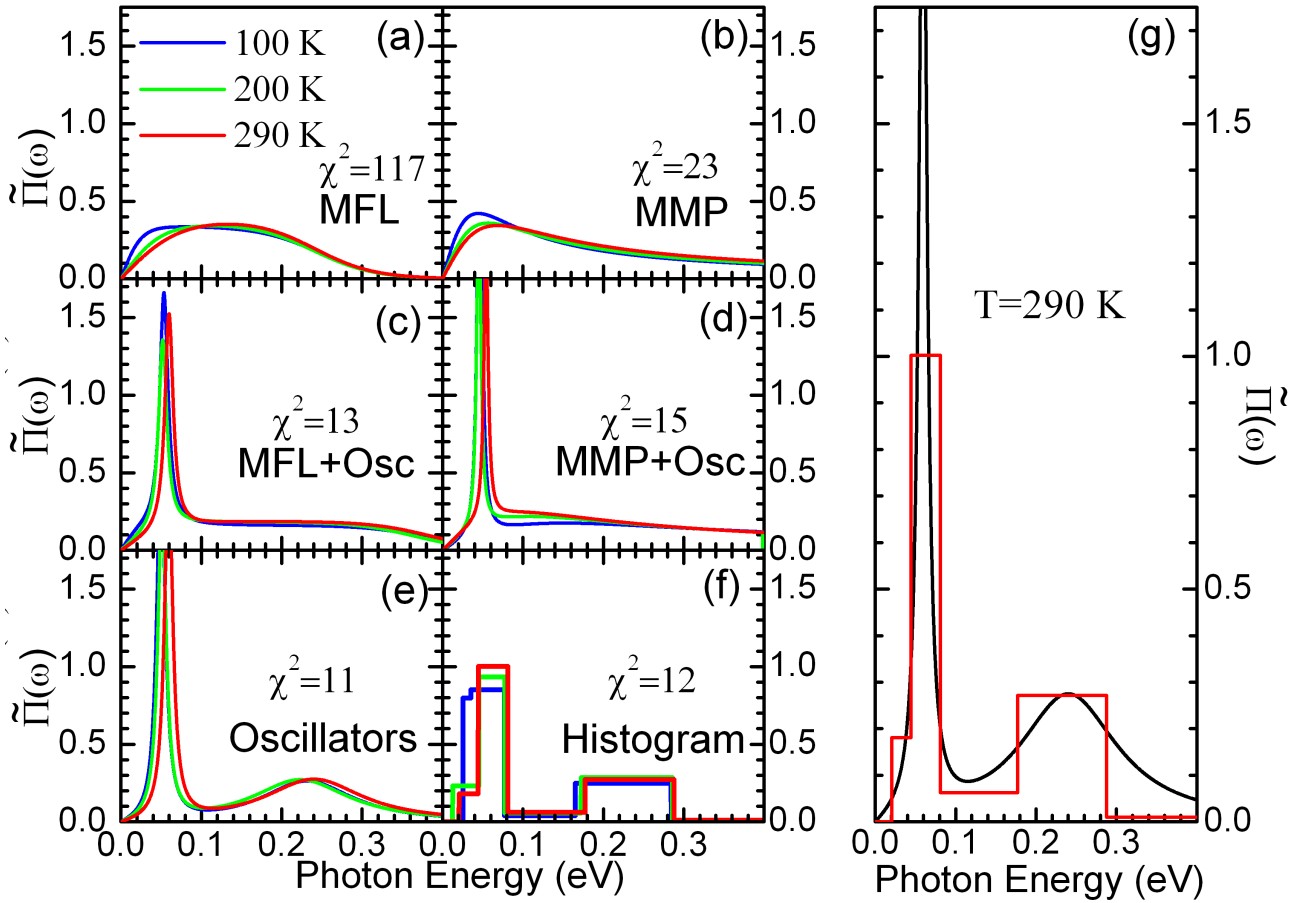


FIG. 5: Comparison of several models. The number of data points over which χ_j^2 is summed (see Eq. 1) is $N = 400$. The quoted values of χ^2 are those for the room temperature spectra. At 100 K these values increase by a factor 1.5 (MFL) and 3.5 (MMP). In contrast, in the oscillator and the histogram model the χ^2 was found to be independent of temperature.

- [2] C.M. Varma, *et al.*, *Phys. Rev. Lett.* **63**, 1996 (1989).
[3] A.J. Millis, H. Monien, D. Pines, *Phys. Rev. B* **42**, 167 (1990).
[4] S.V. Shulga, O.V. Dolgov and E.G. Maksimov, *Physica C* **178**, 266 (1991).
[5] Ar. Abanov, A.V. Chubukov, J. Schmalian, *J. Elec. Spec. Rel. Phen.* **117**, p129 (2000).
[6] P. W. Anderson, *Science* **316**, 1705 (2007).
[7] P. Phillips *Ann. Phys.* **321**, 1634 (2006).
[8] D. N. Basov *et al.*, *Science* **283**, 49-51 (1999).
[9] H.J.A. Molegraaf, C. Presura, D. van der Marel, P.H. Kes, M. Li, *Science* **295**, 2239 (2002).
[10] F. Carbone *et al.*, *Phys. Rev. B* **74**, 064510 (2006).
[11] F. Carbone *et al.*, *Phys. Rev. B* **74**, 024502 (2006).
[12] T. A. Maier, D. Poilblanc, and D. J. Scalapino, *Phys. Rev. Lett.* **100**, 237001 (2008).
[13] $K(\xi, \omega, T) = \int \left[\frac{n(\omega)+f(\epsilon)}{\xi-\epsilon+\omega+i\delta} + \frac{n(\omega)+1-f(\epsilon)}{\xi-\epsilon-\omega-i\delta} \right] d\epsilon$ where $n(\omega)$ and $f(\epsilon)$ are the Bose and Fermi-Dirac distribution functions respectively[15].
[14] W. Goetze, P. Woelfle, *Phys. Rev. B* **6**, 1226 (1972).
[15] P.B. Allen, *Phys. Rev. B* **3**, 305, (1971).
[16] A. Comanac, L. de' Medici, M. Capone, A.J. Millis, *Nature Phys.* **4**, 287, (2008).
[17] E. van Heumen *et al.*, *Phys. Rev. B* **75**, 054522 (2007).
[18] M.R. Norman, A.V. Chubukov, *Phys. Rev. B* **73**, 140501 (2006).
[19] E. van Heumen *et al.*, in preparation.
[20] D. van der Marel *et al.* *Nature* **425**, 271 (2003).
[21] J.L. Tallon *et al.* *phys. stat. sol. (b)* **215**, 531 (1999).
[22] J. Hwang, T. Timusk, E. Schachinger, J.P. Carbotte, *Phys. Rev. B* **75**, 144508 (2007).
[23] J. Hwang, E.J. Nicol, T. Timusk, A. Knigavko, J.P. Carbotte, *Phys. Rev. Lett.* **98**, 207002 (2007).
[24] P.V. Bogdanov *et al.*, *Phys. Rev. Lett.* **85**, 2581 (2000).
[25] A. Lanzara *et al.*, *Nature* **412**, 510 (2001).
[26] W. Meevasana *et al.*, *Phys. Rev. Lett.* **96**, 157003 (2006).
[27] J. Lee *et al.*, *Nature* **442**, 546 (2006).
[28] G. Levy de Castro *et al.*, cond-mat/0703131.
[29] J.F. Zasadzinski *et al.*, *Phys. Rev. Lett.* **87**, 067005 (2001).
[30] A.J. Millis, C.M. Varma, S. Sachdev *Phys. Rev. B* **37**, 4975 (1988).
[31] S.V. Dordevic *et al.*, *Phys. Rev. B* **71**, 104529 (2005).
[32] E. van Heumen, A.B. Kuzmenko, D. van der Marel, submitted to the proceedings of LT25, to be published in *J. Phys.: Conf. Ser.*